The EMBO Journal (2011) 30, 1730–1741 | © 2011 European Molecular Biology Organization | All Rights Reserved 0261-4189/11
www.embojournal.org

THE EMBO JOURNAL

MO25 is a master regulator of SPAK/OSR1 and MST3/MST4/YSK1 protein kinases

Beatrice M Filippi[1,3,*], Paola de los Heros[1], Youcef Mehellou[1], Iva Navratilova[2], Robert Gourlay[1], Maria Deak[1], Lorna Plater[1], Rachel Toth[1], Elton Zeqiraj[1,4] and Dario R Alessi[1,*]

[1]MRC Protein Phosphorylation Unit, College of Life Sciences, University of Dundee, Dundee, UK and [2]Division of Biological Chemistry and Drug Discovery, College of Life Sciences, University of Dundee, Dundee, UK

Mouse protein-25 (MO25) isoforms bind to the STRAD pseudokinase and stabilise it in a conformation that can activate the LKB1 tumour suppressor kinase. We demonstrate that by binding to several STE20 family kinases, MO25 has roles beyond controlling LKB1. These new MO25 targets are SPAK/OSR1 kinases, regulators of ion homeostasis and blood pressure, and MST3/MST4/YSK1, involved in controlling development and morphogenesis. Our analyses suggest that MO25α and MO25β associate with these STE20 kinases in a similar manner to STRAD. MO25 isoforms induce approximately 100-fold activation of SPAK/OSR1 dramatically enhancing their ability to phosphorylate the ion cotransporters NKCC1, NKCC2 and NCC, leading to the identification of several new phosphorylation sites. siRNA-mediated reduction of expression of MO25 isoforms in mammalian cells inhibited phosphorylation of endogenous NKCC1 at residues phosphorylated by SPAK/OSR1, which is rescued by re-expression of MO25α. MO25α/β binding to MST3/MST4/YSK1 also stimulated kinase activity three- to four-fold. MO25 has evolved as a key regulator of a group of STE20 kinases and may represent an ancestral mechanism of regulating conformation of pseudokinases and activating catalytically competent protein kinases.

The EMBO Journal (2011) **30,** 1730–1741. doi:10.1038/emboj.2011.78; Published online 18 March 2011
Subject Categories: signal transduction
Keywords: kinase activation; STE20 kinases; WNK1; WNK4

Introduction

Mouse protein-25 (MO25) was originally identified as an unusually highly conserved protein expressed at the early cleavage stage of mouse embryogenesis (Miyamoto *et al*, 1993; Nozaki *et al*, 1996; Karos and Fischer, 1999). Subsequent studies demonstrated that MO25 operates as a critical scaffolding subunit required for activation and stability of the LKB1 tumour suppressor protein kinase complex, which functions as the master upstream activator of AMPK protein kinases (Boudeau *et al*, 2003a, 2004; Lizcano *et al*, 2004). In mammals, there are two closely related isoforms termed MO25α and MO25β, which share 79% sequence identity that similarly interact and activate LKB1 (Boudeau *et al*, 2003a). MO25α adopts a structure distantly related to armadillo proteins, consisting of seven helical repeats arranged in a distinctive horseshoe shape with a concave surface aligned with highly conserved residues and a less conserved convex surface (Milburn *et al*, 2004). A microRNA (miR-451) whose expression is stimulated by high-energy conditions, promoted growth of gliomas by inhibiting expression of MO25α and thereby inactivating the LKB1 pathway (Godlewski *et al*, 2010).

The LKB1 protein kinase exists as a heterotrimeric protein consisting of MO25 complexed to LKB1 protein kinase and the catalytically inactive pseudokinase STRAD (Baas *et al*, 2003; Boudeau *et al*, 2003a, 2004, 2006). Crystallographic analysis revealed an extensive web of interactions occurring between the N-lobe and helix αC of STRADα (encompassing residues termed Site-A, Site-B and Site-C) and the concave surface of MO25α (Site-1; Zeqiraj *et al*, 2009b; Figure 1A). Moreover, a C-terminal WEF motif on STRADα (Site-D) binds to a pocket at the C terminus convex surface of MO25α (Site-2; Boudeau *et al*, 2003b; Milburn *et al*, 2004; Figure 1A). Despite lacking kinase activity, cooperative interactions with MO25α and ATP force STRADα to adopt a closed conformation resembling that of an active protein kinase (Zeqiraj *et al*, 2009b). This conformation is required for binding LKB1, as crystallographic analysis of the LKB1/STRAD/MO25 complex revealed that STRAD uses active site elements (activation and substrate binding loops) to engage LKB1 as a pseudosubstrate (Zeqiraj *et al*, 2009a). Mutant forms of STRADα that are unable to bind MO25α and ATP, and are predicted to adopt an open-inactive conformation, fail to activate LKB1 (Zeqiraj *et al*, 2009b).

STRADα and STRADβ isoforms are members of the STE20 protein kinases consisting of germinal centre kinases (GCKs) that have an N-terminal kinase domain and P21-activated kinases (PAKs) that have a C-terminal kinase domain (Dan *et al*, 2001; Manning *et al*, 2002; Figure 1B). Many members of the STE family kinases function as upstream components in signal-transduction pathways controlling a wide range of biological processes. STRAD isoforms belong to the GCK group and are most closely related to SPAK and OSR1 protein kinases that are important regulators of ion homeostasis and

*Corresponding authors. BM Filippi or DR Alessi, MRC Protein Phosphorylation Unit, College of Life Sciences, University of Dundee, Dundee DD1 5EH, UK. Tel.: +1 416 5811 7697; Fax: +1 416 5811 7697; E-mail: bfilippi@uhnresearch.ca or Tel.: +44 138 234 5602; Fax: +44 138 222 3778; E-mail: d.r.alessi@dundee.ac.uk
[3]Present address: University Health Network, MaRS Centre, Toronto Medical Discovery Tower, Room 10-706, 101 College St Toronto, Canada M5G 1L7.
[4]Present address: Samuel Lunenfeld Research Institute, Mount Sinai Hospital, 600 University Avenue, Room 1090, Toronto, Ontario, Canada M5G 1X5

Received: 15 November 2010; accepted: 23 February 2011; published online: 18 March 2011

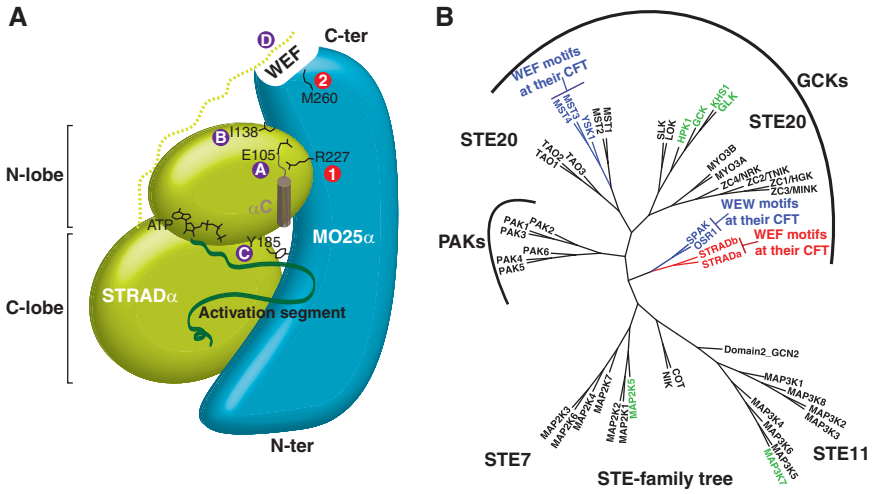

Figure 1 Conservation of the STRAD–MO25 interaction among the STE-family kinases. (**A**) Schematic representation of the STRAD–MO25 interaction based on the crystal structure (PDBID 3GNI; Zeqiraj *et al*, 2009b). Highlighted are key interaction sites referred to in this study as sites 1 and 2 on MO25α (in red) and sites A, B, C and D on STRADα (in purple). (**B**) Neighbour-joining distance tree of the human STE kinase family (STE20, STE7, STE11; Manning *et al*, 2002). The STE20 kinases that possess all four conserved putative MO25α binding sites are highlighted in blue and those with three conserved sites in green. STRADα and STRADβ are highlighted in red. CFT, C-terminal flanking tail of kinase domain.

blood pressure and are activated by the WNK protein kinases (Vitari *et al*, 2005; Richardson and Alessi, 2008; Rafiqi *et al*, 2010).

In *S. cerevisiae*, three kinases (Elm1, Pak1 and Tos3) resemble LKB1 and act as alternative upstream kinases to activate the AMPK orthologue SNF1 (Elbing *et al*, 2006; Hedbacker and Carlson, 2008). Elm1, Pak1 and Tos3 are likely to be regulated in a different manner to mammalian LKB1, as there are no obvious orthologues of a pseudokinase resembling STRAD. However, yeast do possess orthologues of MO25, termed HYM1 in *S. cerevisiae* or pMO25 in *S. pombe*, but no interactions with the SNF1 pathway have been reported, suggesting that HYM1/pMO25 have other roles. Consistent with this, Hym1 was found to interact with an active orthologue of the mammalian MST-STE20 kinase (Kic1; Bidlingmaier *et al*, 2001; Nelson *et al*, 2003). HYM1 and Kic1 regulate transcriptional activity as well as morphogenesis by activating an NDR kinase (cbk1; Bidlingmaier *et al*, 2001; Nelson *et al*, 2003). Similarly, in *S. pombe*, pMO25 controls morphogenesis by interacting with an MST-STE20 kinase orthologue (Nak1) and regulating activation of an NDR kinase orthologue (Orb6; Kanai *et al*, 2005). Recently, pMO25 has been shown to have an auxiliary role in regulating cell separation by interacting with another MST kinase termed Ppk11 (Goshima *et al*, 2010). Perhaps connecting the studies in the yeast and the mammalian systems, human MST4 was reported to interact with the LKB1 complex by virtue of its ability to bind MO25 (ten Klooster *et al*, 2009). This was proposed to enable MST4 to phosphorylate ezrin and control cellular brush border formation (ten Klooster *et al*, 2009).

In mammalian systems, all the data accumulated thus far point to the biological roles of MO25 being mediated via its ability to regulate LKB1. Here we provide evidence that MO25α has roles beyond activating LKB1 in mammalian cells. We demonstrate that in addition to binding STRADα/STRADβ, MO25 isoforms also interact in a similar manner with at least five other STE20 kinases, namely SPAK, OSR1 (regulators of ion homeostasis and blood pressure) and MST3, MST4, YSK1 (regulators of morphogenesis and polarity). Remarkably, SPAK as well as OSR1 are activated approximately 100-fold by binding to MO25 isoforms, whereas MST3, MST4 and YSK1 are activated three- to four-fold. We also provide evidence that knockdown of MO25α suppresses phosphorylation and activation of the NKCC1 ion cotransporter mediated by SPAK and OSR1. Our findings indicate that MO25 has evolved as a master activator of several STE20 kinases and we discuss the idea that binding to MO25 may have evolved as an ancestral mechanism to activate STE20 pseudokinases and kinases.

Results

MO25 interacting residues on STRAD are conserved in other STE20 kinases

There are four groups of surface-exposed residues on STRADα that interact with MO25 and we have termed them Sites A, B, C and D (Figure 1A). Mutation of key residues within each of these sites abolishes or markedly inhibits STRADα binding to MO25α (Zeqiraj *et al*, 2009b). Sequence analysis of all human STE20 kinases as well as related STE7 and STE11 kinases (48 kinases in total) suggested that five kinases had all four conserved sites (SPAK, OSR1, MST3, MST4 and YSK1), and six kinases had three conserved sites (HPK1, GCK, KHS1, KHS2, MAP2K5 and MAP3K7; Figure 1B, Supplementary Table I, Figures S1 and S2).

MO25α stimulates activity of five STE20 kinases that posses conserved MO25α binding sites

We next determined how the addition of MO25α influenced the kinase activity of 26 representative STE kinases that we were able to clone, express, affinity purify and measure kinase activity (Figure 2A). MO25α induced significant activation of the five STE20 kinases that possess all four conserved putative MO25α binding sites (SPAK, OSR1, MST3, MST4 and YSK1), but did not activate any of the other

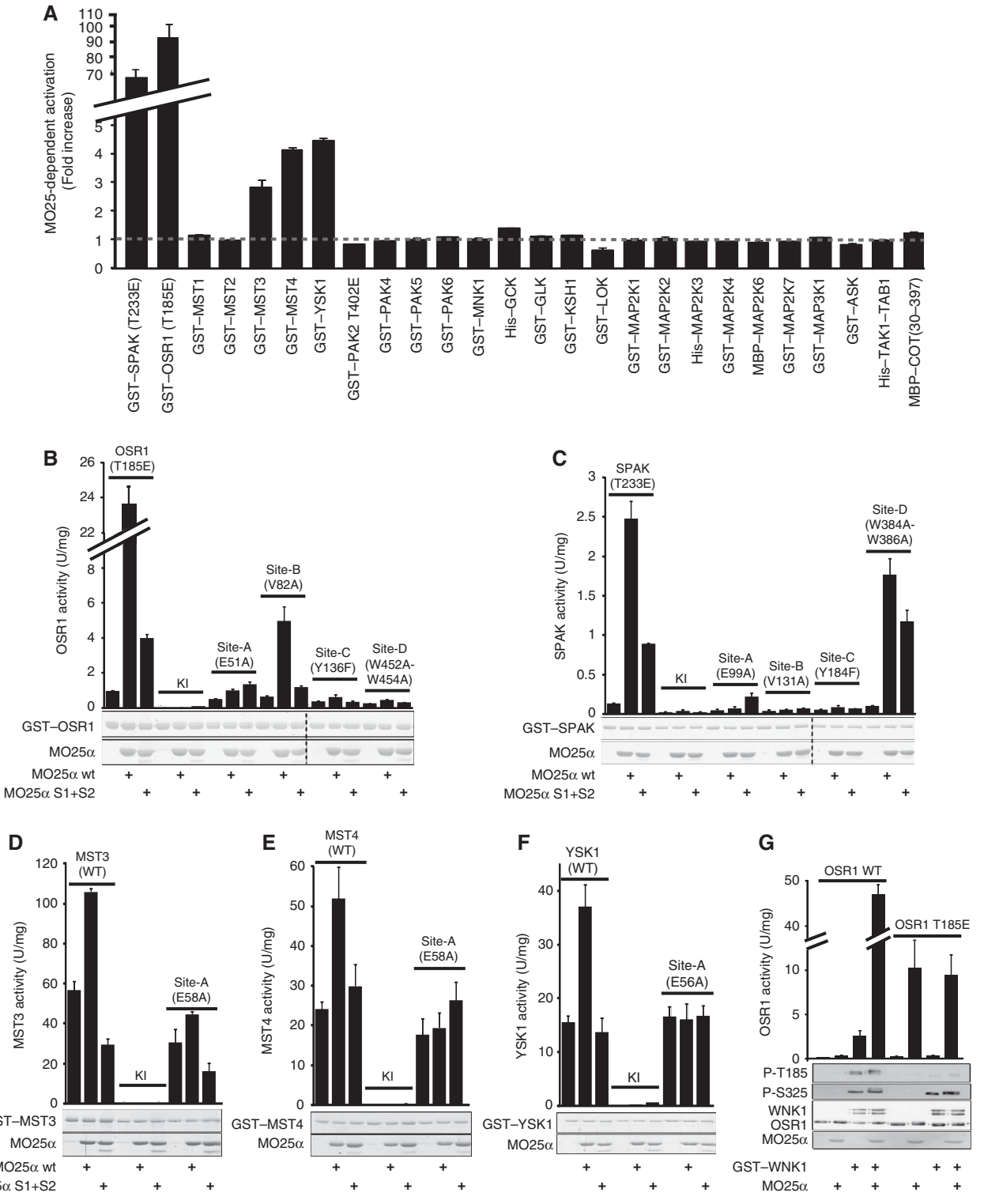

Figure 2 Activation of various STE20 kinases by MO25α. (**A**) The indicated kinases were assayed in the absence or presence of five-fold molar excess of wild-type MO25α. The activity in the presence of MO25α is reported relative to the activity measured in the absence of MO25α. Assay conditions and substrates for each kinase are reported in Supplementary Table II. Assays were undertaken in triplicate and data presented as mean ± s.d. (**B**–**F**) As in (**A**) except the wild-type or indicated STE20 GST-tagged kinase mutants purified from HEK293 cells were employed. Activities were measured in the presence or absence of MO25α purified from bacteria and are presented in U/mg, as mean ± s.d. (**G**) GST–OSR1 (0.22 μM) WT and T185E were activated with GST–WNK1 catalytic domain using an *in vitro* cold reaction for 20 min at 30°C in the presence or absence of 1 μM WT-MO25α. The catalytic activity of OSR1 was then assayed by adding the CATCHtide and [γ^{32}P]ATP for another 15 min at 30°C. The activity is presented as U/mg ± s.d. The phosphorylation status of the T-loop (T185) and the S-motif (S235) are also shown. The GST blot shows the total amount of GST–OSR1 and GST–WNK used for the reaction, and MO25α is visualised by Ponceau staining. Dotted line indicates that these samples were run on separate gels.

kinases tested (Figure 2A). Strikingly, MO25α induced between 70- and 100-fold activation of a mutant of SPAK and OSR1, in which the T-loop activating residue phosphorylated by WNK isoforms was changed to Glu to mimic phosphorylation (Figure 2A and Supplementary Figure S3). The activity of MST3, MST4 and YSK1 was stimulated three- to four-fold by addition of MO25α (Figure 2A and Supplementary Figure S4).

MO25α possesses two conserved STRADα interacting sites, Site-1 and Site-2 (Figure 1), which when mutated individually reduce its affinity for STRADα and when changed together abolish the MO25-STRAD interaction (Zeqiraj *et al*, 2009b). Combined mutation of Site-1 and Site-2 virtually abolished the ability of MO25α to activate OSR1 (Figure 2B), SPAK (Figure 2C), MST3 (Figure 2D), MST4 (Figure 2E) and YSK1 (Figure 2F). Individual mutation of Site-1 and Site-2 partially reduced the ability of MO25α to activate these kinases, with Site-1 having the biggest effect (Supplementary Figures S3A, C and S4A, C, E). MO25α activated SPAK and OSR1 (Supplementary Figure S3B, D) and MST3, MST4 and YSK1 (Supplementary Figure S4B, D, F) in a dose-dependent manner with near-maximal activation observed with approximately 10-fold molar excess MO25α over each STE20 kinase. The MO25β isoform activated OSR1, SPAK and MST4 to the same extent as MO25α, with combined mutation of Site-1 and Site-2 inhibiting activation (Supplementary Figure S5).

We next verified how mutations of Sites A to D (Figure 1) that are equivalent to those that inhibit binding of STRADα to MO25α affected activation of SPAK, OSR1, MST3, MST4 and YSK1. Strikingly, mutation of Site-A did not affect basal kinase activity, but virtually abolished MO25α-induced activation (Figure 2B–F). Individual mutations of Sites B, C and D also inhibited to varying extents the activation of OSR1 (Figure 2B), SPAK (Figure 2C), MST3 (Supplementary Figure S6A), MST4 (Supplementary Figure S6B) and YSK1 (Supplementary Figure S6C) by MO25α.

Previous studies have shown that SPAK and OSR1 require T-loop phosphorylation by WNK kinases in order to be active (Vitari *et al*, 2005; Zagorska *et al*, 2007). We observed that MO25α does not activate bacterially expressed OSR1 that is not phosphorylated at its T-loop by WNK1 (Figure 2G). Phosphorylation of the T-loop residue of OSR1 or its mutation to Glu to mimic phosphorylation is required for triggering activation by MO25α (Figure 2G). Interestingly, in the absence of MO25α, phosphorylation of the T-loop of OSR1 or its mutation to Glu only activates OSR1 to less than 10% of the activity observed in the presence of MO25α. Thus, phosphorylation of the activation loop by upstream kinases is necessary for activation of SPAK/OSR1, but MO25 is required for full activation of these kinases.

Binding of MO25α to SPAK, OSR1 and MST4

Consistent with two major binding surfaces between STRADα and MO25α, binding data from surface plasmon resonance (SPR) studies between these proteins could be fitted to a two-site-binding equation (Hill slope of 0.4), with K_{d1} calculated as 0.012 μM and K_{d2} was measured as 2.5 μM (Zeqiraj *et al*, 2009b). We analysed in a similar way the interaction of SPAK, OSR1 and MST4 with MO25α using SPR (Figure 3). This revealed that wild-type MO25α interacted with SPAK (Figure 3A), OSR1 (Figure 3B) and MST4 (Figure 3C) and,

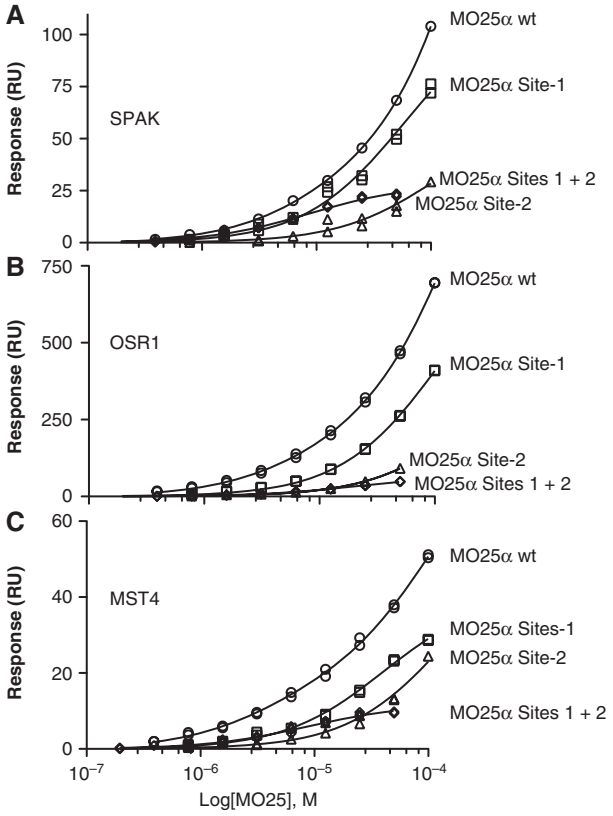

D

Target	Analyte	K_d1 (μM)	K_d2 (μM)
OSR1	MO25 (WT)	5.7±1.5	200±52
	MO25 (Site-1)	116±5.5	ND
	MO25 (Site-2)	265±98	ND
	MO25 (Sites 1+2)	ND	ND
SPAK	MO25 (WT)	8.2±1.8	457±260
	MO25 (Site-1)	58±9	ND
	MO25 (Site-2)	116±39	ND
	MO25 (Sites 1+2)	ND	ND
MST4	MO25 (WT)	3.8±0.9	125±42
	MO25 (Site-1)	40.3±3	ND
	MO25 (Site-2)	145±30	ND
	MO25 (Sites 1+2)	ND	ND
		K_d1 (μM)	K_d2 (μM)
STRADα *	MO25 (WT)	0.051±0.0002	5.1±0.02
	MO25 (Site-1)	ND	0.8±0.005
	MO25 (Site-2)	0.082±0.0006	2.3±0.001
	MO25 (Sites 1+2)	ND	ND

Figure 3 SPAK, OSR1, MST3 and MST4 interact with MO25 with low micromolar affinity. Binding of SPAK (**A**), OSR1 (**B**) and MST4 (**C**) to MO25α was assessed in an SPR BIAcore assay by immobilising these kinases to a CM5 sensor chip, and allowing the indicated forms of MO25α to bind over 30 s by injecting different concentrations over a range of 200 nM to 100 μM in the presence of 0.1 mM ATP and 1 mM $MgCl_2$. Response levels for specific binding of MO25α to the STE20 kinases is plotted against MO25α concentrations (log scale), using, where appropriate, a variable slope model to determine the Hill slope from the data. (**D**) Equilibrium binding constants (K_d) were calculated from a saturation binding model for specific binding that follows the law of mass action (see Materials and methods section). Forms of MO25, SPAK and OSR1 employed in this study were purified from bacteria, and the GST purification tag was removed before SPR analysis (Supplementary Table S2). His-tagged MST4 was purified from insect cells (Supplementary Table S2). ND, not determined. Gels of the purified proteins used for SPR are shown in Supplementary Figure S15G & H. Asterisk indicates STRAD/MO25 K_d values are taken from (Zeqiraj *et al*, 2009b).

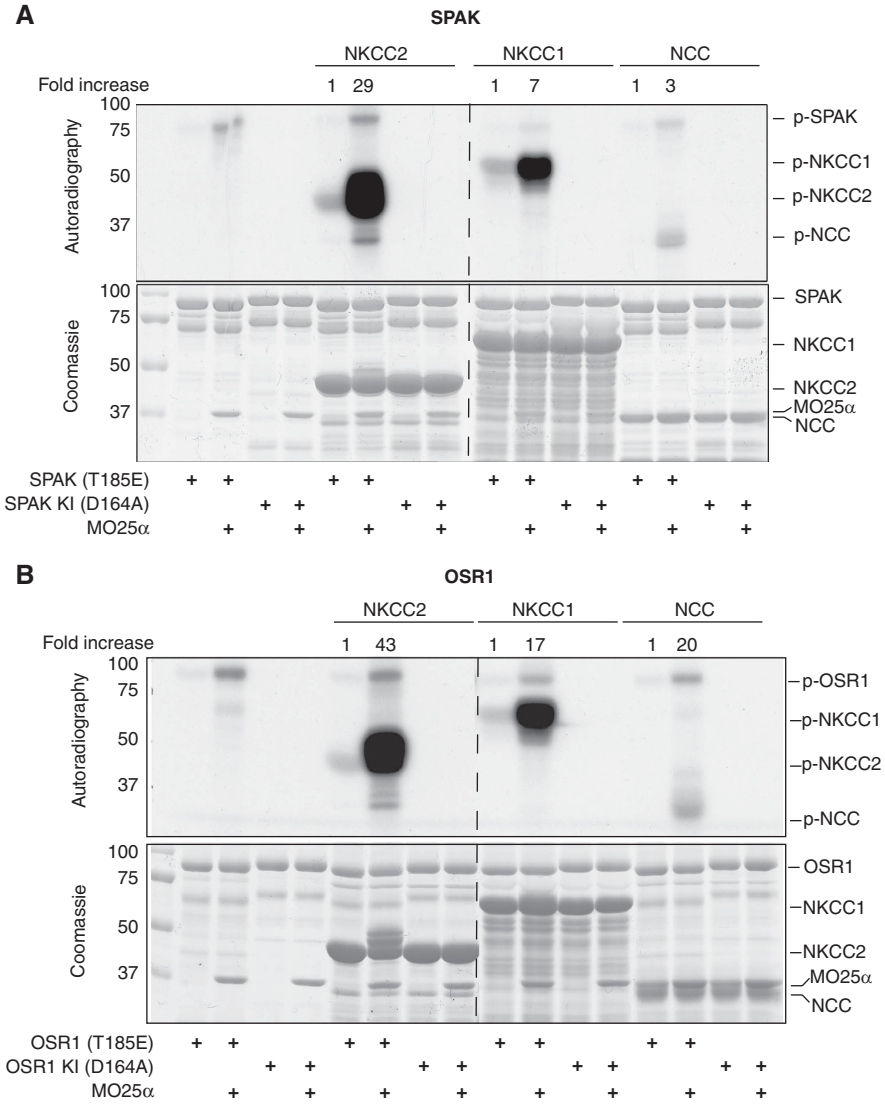

Figure 4 MO25α dramatically enhances phosphorylation of ion cotransporters by SPAK and OSR1. Fragments of ion cotransporters that encompass the known SPAK/OSR1 phosphorylation sites (GST-NKCC2[1-174], GST-NKCC1[1-260] and GST-NCC[1-100]) were expressed in *E. coli*. These were incubated with the active SPAK[T233E] (**A**) and OSR1[T185E] (**B**), as well as the kinase-inactive (KI) forms of these enzymes, in the absence or presence of a 10-molar excess of MO25α. Reactions were performed in the presence of Mg-[γ^{32}P]ATP for 20 min. Phosphorylation of substrates was analysed following electrophoresis and autoradiography of the Colloidal blue-stained bands, which were subsequently isolated and quantified by Cerenkov counting. The fold increase in phosphorylation observed in the presence of MO25α is also indicated. Similar results were obtained in two separate experiments. Dotted lines between autorads and gels indicate that these were undertaken on separate gels.

analogous to STRADα, binding data could be fitted to a two-site-binding equation (Hill slope of 0.6–0.7). The K_{d1} values were between 3 and 8 μM and K_{d2} constants were much higher ~125 to 450 μM (Figure 3D). Consistent with the two-site-binding interaction being mediated through Site-1 and Site-2, mutation of either MO25 binding site resulted in a binding curve that could be fitted with a one site-binding equation (Hill slope of 1), and the binding affinity of these single-site MO25 mutants to SPAK, OSR1 and MST4 was markedly reduced (Figure 3). As expected, the double MO25α Site-1 and Site-2 mutants failed to significantly interact with these STE20 kinases (Figure 3).

Effect of MO25α on phosphorylation of ion cotransporters by SPAK and OSR1

There are three known physiological substrates for SPAK/OSR1, namely the ubiquitously expressed NKCC1 ion cotransporter and the kidney-specific NCC and NKCC2 ion cotransporters that are targets for thiazide and loop diuretic hypertension drugs (Richardson and Alessi, 2008). SPAK and OSR1 phosphorylate these ion cotransporters at a cluster of mainly Thr residues within the N-terminal intracellular domain, leading to higher rates of ion transport activity (Richardson and Alessi, 2008). We therefore investigated the effect that MO25α had on the ability of SPAK (Figure 4A) and OSR1 (Figure 4B) to phosphorylate these ion cotransporters and found that MO25α hugely enhanced phosphorylation of NKCC1, NKCC2 and NCC (Figure 4). We also mapped residues phosphorylated on these ion cotransporters by OSR1 in the presence of MO25α *in vitro* (Supplementary Figure S7, S8 and S9). Interestingly, for the three ion cotransporters we mapped phosphorylation sites that have been reported *in vivo*. In the case of NKCC2, in addition to the previously observed Thr95 and Thr100 resi-

dues (Richardson *et al*, 2011), two additional phosphorylated residues, namely Thr118 and Ser120, were identified (Supplementary Figure S7). Thr118 (Gimenez and Forbush, 2005; Ponce-Coria *et al*, 2008) has been reported to be phosphorylated *in vivo* in response to hypotonic stimuli that activate SPAK/OSR1 (Richardson *et al*, 2011; Supplementary Figure S7). In the case of NKCC1, in addition to the previously reported sites (Thr203, Thr107, Thr212; Vitari *et al*, 2006), two other sites were observed (Thr217 and Thr230), both of which have been reported to be phosphorylated *in vivo* (Darman and Forbush, 2002; Supplementary Figure S8). In the case of NCC, in addition to the previously identified sites (Thr46, Thr55 and Thr60; Richardson *et al*, 2008), we observed phosphorylation of residue Ser73, also a characterised hypotonic-induced *in vivo* phosphorylation site (Yang *et al*, 2007; Supplementary Figure S9). Thus, due to the enhanced MO25-dependant activation of OSR1 we were able to identify new NKCC1/2 and NCC phosphorylation sites, as well as confirm phosphorylation sites that were previously attributed to the activity of SPAK and OSR1 *in vivo* (Supplementary Figure S10).

siRNA knockdown of MO25α reduced SPAK/OSR1-mediated phosphorylation of NKCC1 in vivo

To study whether interaction of SPAK/OSR1 with MO25α is important for regulating the phosphorylation of endogenous NKCC1, we knocked down expression of MO25α by ~75% in HEK293 cells using two separate siRNA oligonucleotides (Figure 5A and Supplementary Figure S11). We then investigated how this impacted on the phosphorylation of NKCC1 induced by hypotonic low-chloride conditions at residues phosphorylated by SPAK/OSR1 (Thr203/Thr207/Thr212; Vitari *et al*, 2006). Consistent with the siRNA probes lowering MO25α levels sufficiently to ablate its physiological functions, knockdown of MO25α suppressed phosphorylation of AMPK catalytic subunit at Thr172 (Figure 5A and Supplementary Figure S11) that is phosphorylated by the LKB1/STRAD/MO25 complex (Alessi *et al*, 2006). In cells treated with scrambled siRNA, as expected, hypotonic low-chloride conditions induced significant phosphorylation of NKCC1, which was accompanied by increased phosphorylation of SPAK/OSR1 at the T-loop and S-motif residues that are phosphorylated by WNK1 (Figure 5A and Supplementary Figure S11). However, in cells in which expression of MO25α was reduced, significantly lower phosphorylation of NKCC1 in response to hypotonic low-chloride conditions was observed (Figure 5A and Supplementary Figure S11). Re-expression of MO25α in cells treated with siRNA targeting MO25α rescued this effect and increased the basal as well as the hypotonic low-chloride-induced phosphorylation of NKCC1 to the level observed in control cells (Figure 5A). Consistent with reduced phosphorylation of NKCC1, knockdown of MO25α lowered NKCC1 activity assessed by measuring the ability of cells to uptake $^{86}Rb^{+}$ in a bumetanide (specific NKCC1 inhibitor)-sensitive manner. Reduction of MO25α lowered both the basal as well as the stimulated activity observed in response to hypotonic low-chloride conditions (Figure 5B).

Knockdown of MO25α did not significantly affect the phosphorylation of OSR1 and SPAK at the T-loop and S-motif (Figure 5A and Supplementary Figure S11), suggesting that MO25α binding does not promote SPAK/OSR1 phosphorylation by WNK1. Consistent with this, *in vitro* phosphorylation assays of OSR1 by WNK1 revealed that addition of MO25α did not influence WNK1-mediated phosphorylation of the T-loop and S-motif (Supplementary Figure S12).

Discussion

The key finding of this study is that MO25α in mammalian cells is likely to have a major role in regulating the activity of at least five other STE20 kinases (SPAK, OSR1, MST3, MST4 and YSK1), and thereby have roles beyond controlling the LKB1 tumour suppressor complex. Our findings that MO25 isoforms interact and activate MST3, MST4 and YSK1 are in agreement with the elegant genetic analyses indicating that yeast MO25 orthologues control the MST kinase–NDR kinase signalling network that regulate transcription, development and morphogenesis (Bidlingmaier *et al*, 2001; Nelson *et al*, 2003; Kanai *et al*, 2005). Mammalian MST3 kinase triggers the activation of the NDR1 and NDR2 kinases by phosphorylating these enzymes at their hydrophobic motif, triggering autophosphorylation of the T-loop (Stegert *et al*, 2005). Recently, the ability of fission yeast pMO25 to regulate the function of the MST/STE20 kinase homologue Ppk11 during cell morphogenesis was impaired by mutating a C-terminal WDF motif that corresponds to Site-D on the STRADα/MO25α interface (Goshima *et al*, 2010; Figure 1A). Similarly, we find that mutation of the equivalent Site-D residues in SPAK/OSR1 (Figure 2B and C) or MST3/MST4 and YSK1 (Supplementary Figure S6) also markedly suppresses activation of these kinases by MO25α.

Recent work has also identified an interesting microRNA termed miR-451 that suppresses MO25α expression and controls glioma cell proliferation, migration and responsiveness to glucose deprivation (Godlewski *et al*, 2010). The effects that miR-451 had on cells were interpreted to be mediated through inhibition of the LKB1 tumour suppressor complex. However, our findings suggest that some of the striking effects of miR-451 could be mediated in part, independently of LKB1 through inhibition of STE20 kinases. Although in this study we have focused on five STE20 kinases that are activated by MO25α, it is possible that other kinases we have not tested are also activated by MO25α. Moreover, MO25α could interact with other STE20 kinases that we have analysed in Figure 2A, without activating them directly under conditions we tested.

The difference in affinity of MO25 for STRAD (low nanomolar range) and other STE20 kinases (low micromolar range) may be indicative of different modes of MO25-dependent regulation. In the case of MO25 interacting with STRAD the key role of this regulatory complex is to activate the LKB1 kinase, which remains constitutively active within this complex. By contrast, regulation of SPAK, OSR1, MST3, MST4 and YSK1 may require a more responsive dynamic on-off regulation, which could be better mediated by lower-affinity interaction with MO25. The low micromolar interaction between MO25 isoforms and its novel binding partners analysed in this study is likely to account for why immunoprecipitation of endogenous forms of SPAK, OSR1, MST3, MST4 and YSK1 does not result in marked co-immunoprecipitation of endogenous MO25α (BMF data not shown), as dissociation of these proteins would occur during the time required to lyse cells and undertake the immunoprecipitations.

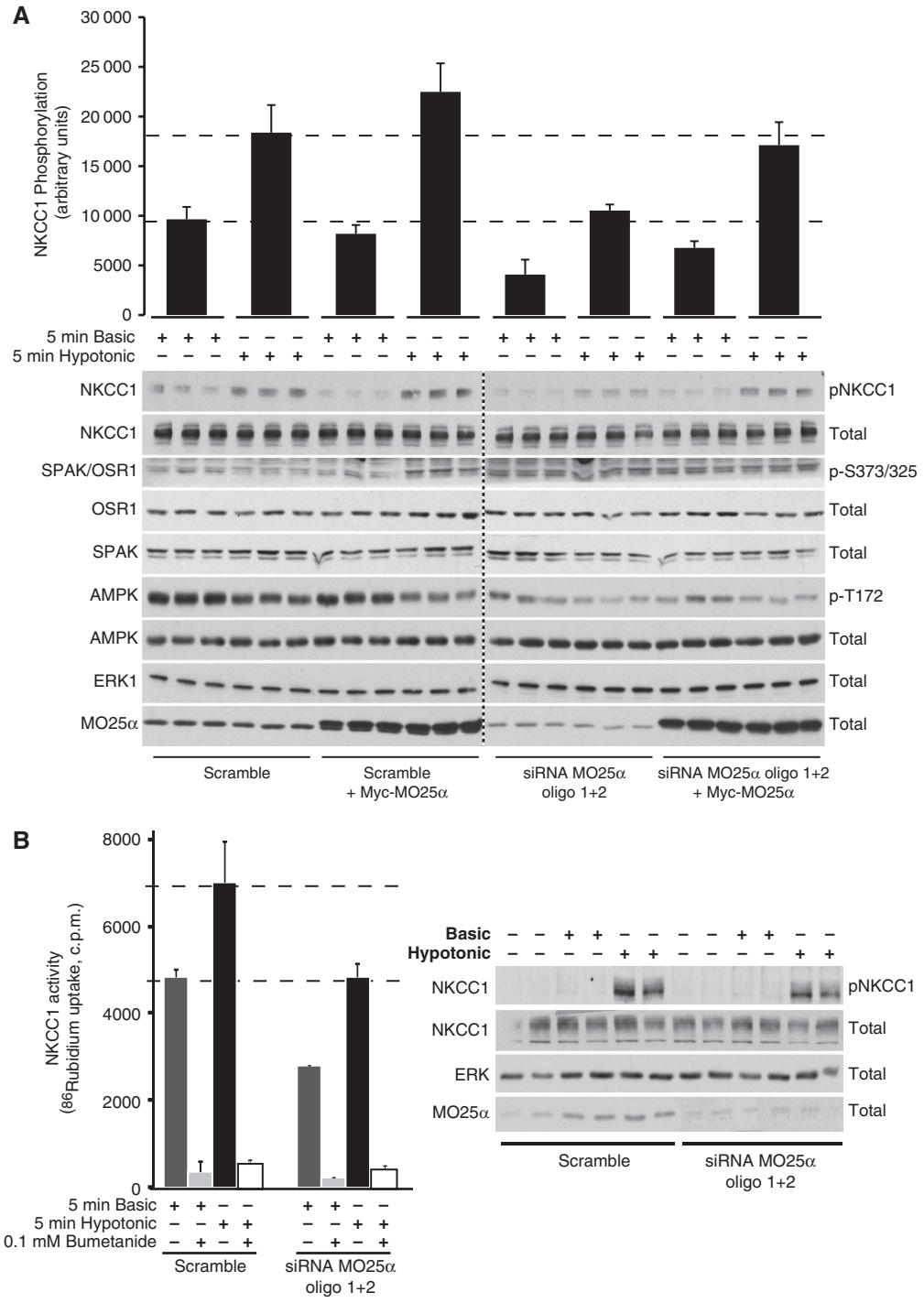

Figure 5 Dependence of NKCC1 phosphorylation and activation on MO25α. HEK293 cells were transfected with the indicated siRNA oligonucleotides for 72 h in the absence or presence of overexpression of Myc-MO25α. siRNA sequences target the non-coding region (3′ UTR) of the MO25α gene and do not affect the expression of Myc-MO25α under the pCMV vector promoter. (**A**) Cells were stimulated with basic or hypotonic low-chloride conditions for 5 min. Cells were lysed and subjected to immunoblot analysis with the indicated total and phosphospecific antibodies. Samples from each lane were derived from a separate dish of independently transfected cells. Similar results were obtained in two separate experiments. A quantification of NKCC1 phosphorylation by using fluorophore-conjugated secondary antibodies (Molecular Probes), followed by visualisation using an Odyssey® LI-COR imaging system is also shown. pNKCC1 antibody recognises NKCC1 phosphorylated at the three residues (Thr203, Thr207 and Thr212) phosphorylated by SPAK and OSR1 (Vitari *et al*, 2006). (**B**) Cells were incubated with either basic or hypotonic low-chloride buffers for 5 min in the presence of 1 mM Ouabain (specific Na^+/K^+ ATPase inhibitor) and in the presence or absence of 0.1 mM Bumetanide (specific NKCC1 inhibitor). Cells were then incubated in isotonic uptake buffer containing ^{86}Rb, and uptake was allowed to proceed for 5 min. Cells were rapidly washed on ice, lysed, and ^{86}Rb taken into cells was quantified by scintillation counting. Observed ^{86}Rb uptake (c.p.m.) for each condition is plotted. The activity assay results are all presented as the mean ^{86}Rb uptake c.p.m. ± s.d. for triplicate samples. The cell extracts were also subjected to immunoblot analysis with the indicated antibodies. Similar results were obtained in three separate experiments. Dotted line between immunoblots indicates that these were undertaken on separate gels.

Nevertheless, using an overexpression approach we were able to observe co-immunoprecipitation of MO25α with MST4, YSK1 and SPAK in HEK293 cells which was inhibited following mutation of Site-1 and Site-2 in MO25α (Supplementary Figure S13). In the case of STRADα, its interaction with MO25α is greatly stabilised by the binding to LKB1 that interacts with both STRAD and MO25α (Boudeau *et al*, 2003a, 2004; Zeqiraj *et al*, 2009a). Our co-immunoprecipitation studies indicate that the equivalent subunits to LKB1 that lock STE20 kinases in a stable complex with MO25α may not exist. Compared with STRADα, expression of MO25 isoforms is less variable among tissues (Supplementary Figure S14). In kidney tissues, where the SPAK/OSR1 has a key role in regulating blood pressure, MO25α and MO25β are highly expressed, whereas STRADα is expressed at low levels (Supplementary Figure S14). Further evidence suggesting MO25α has functions beyond controlling LKB1, result from previous studies indicating that STRADα was destabilised and barely detected in LKB1-deficient cells, under conditions in which MO25α and MO25β expression was unaffected (Hawley *et al*, 2003). In future work it would be interesting to investigate how assembly of different MO25–STE20 kinase complexes is regulated in various tissues including the kidney, and how the expression of these subunits is coordinated. It would also be interesting to study whether disruption of complexes of SPAK and OSR1 with MO25 could be linked to the development of hypertension.

Our data suggest that the molecular mechanism by which MO25α binds to SPAK/OSR1 and MST3/MST4/YSK1 is similar to how it interacts with STRADα, as mutations on the residues of MO25 that inhibit binding to STRADα also suppress interaction with these STE20 kinases (Figure 2). Similarly, mutating the conserved residues on SPAK/OSR1 and MST3/MST4/YSK1 corresponding to sites of STRADα that interact with MO25α, inhibited interaction with MO25α (Figure 2). In the case of STRADα, binding of MO25α stabilises it in an active conformation that can bind and stimulate LKB1 (Zeqiraj *et al*, 2009b). It is likely that MO25α binding to SPAK/OSR1 and MST3/MST4/YSK1 also promotes these enzymes to adopt an active conformation as MO25α stimulates the intrinsic kinase activity of these enzymes. In the MO25α–STRADα complex, STRADα attains an active conformation and the substrate-binding site of STRADα is fully accessible and freely available to bind LKB1 as a pseudosubstrate (Zeqiraj *et al*, 2009a). Assuming that the mode of interaction and the mechanism of activation of MO25 and STE20 kinases are similar, the substrate binding site of STE20 kinases should be accessible to their substrates even when these kinases are bound to MO25. In this manner, MO25 isoforms would not need to dissociate from the STE20 kinase in order for these enzymes to access their substrates.

STRADα adopts an active conformation when it interacts with MO25α and ATP and is aided by a naturally occurring phospho-mimicking residue (D232) on its T-loop to assume this active conformation (Zeqiraj *et al*, 2009b). Similar to most protein kinases, SPAK/OSR1 and MST3/MST4/YSK1 require T-loop phosphorylation in order to be activated. This is also emphasised by the finding that MO25α does not activate OSR1 that is not phosphorylated at its T-loop residue (Figure 2G). Moreover, phosphorylation of the T-loop residue of OSR1 only activates OSR1 to a small extent compared with activation achieved following binding to MO25α (Figure 2G). It is likely that phosphorylation of the T-loop promotes the active conformation of SPAK/OSR1 and MST3/MST4/YSK1 kinases, and MO25α binding stabilises this active conformation that results to full kinase activation. Such mechanism of activation by T-loop phosphorylation and allosteric potentiation by scaffold proteins is not unprecedented and has been described for CDK-cyclin and EGFR–EGFR dimers (Jefferey *et al*, 1995; Zhang *et al*, 2006). STRAD and MO25 interactions have general resemblance to the interactions of CDKs with cyclins and in both cases the interactions are centred on the regulatory helix αC that is critical for kinase activation (Zeqiraj *et al*, 2009b).

The catalytic domain of OSR1[T185E] has been crystallised and found to adopt a curious inactive conformation (Villa *et al*, 2008; Lee *et al*, 2009), accounting for the low-activity state of this enzyme. It would be fascinating to crystallise the complex of OSR1 or SPAK with MO25α to determine how MO25α binding increases SPAK/OSR1 kinase activity by ~100-fold. The structure of MST3 kinase in the active conformation has also recently been reported (Ko *et al*, 2010) as has the structure of the inactive MST4 (Record *et al*, 2010). It would also be interesting to co-crystallise MO25α with these MST kinases to establish how MO25α activates these. The LKB1 complex reportedly interacts with the MST4 kinase via MO25 (ten Klooster *et al*, 2009). Our data suggest that the same residues on MO25α that bind to STRAD are also involved in binding to MST4 (Figure 2E). Thus, available data on how MO25α binds to STRADα and MST4 suggest that it would not be possible for MO25 to interact simultaneously with both STRAD/LKB1 as well as MST4.

Until now, SPAK and OSR1 have been studied in the absence of MO25α and have been found to possess very low kinase activity making it hard to identify new substrates. The discovery that MO25α hugely activates SPAK/OSR1 will assist in the identification of new substrates of these enzymes. As SPAK/OSR1 activate the NCC and NKCC2 ion cotransporters, which are the drug targets for widely used thiazide and loop diuretic hypertensive drugs, there is excitement about the possibility of SPAK and OSR1 inhibitors being deployed for the treatment of hypertension. Consistent with the idea that such compounds would reduce blood pressure, knockin mice expressing a T-loop mutant of SPAK that cannot be activated by WNK isoforms, display markedly reduced blood pressure (Rafiqi *et al*, 2010), a finding that has recently been confirmed in SPAK knockout mice (Yang *et al*, 2010). Screening for SPAK/OSR1 inhibitors has been hampered by the poor activity of the SPAK and OSR1 recombinant enzymes. In future, we recommend that screening for SPAK/OSR1 inhibitors is undertaken with the SPAK/OSR1/MO25α complex rather than the isolated kinases. Using the OSR1/MO25α complex we have also identified a number of novel *in vitro* phosphorylation sites on NKCC1 (Thr217, Thr230), NKCC2 (Thr118, Ser120) and NCC (Ser73), which were not observed in previous phosphorylation site analysis undertaken with isolated SPAK and OSR1. Our new data suggest that these residues are likely to represent direct phosphorylation sites. In Supplementary Figure S10, we include a sequence alignment of the NKCC1, NKCC2 and NCC ion cotransporters summarising positions of all reported *in vitro* and *in vivo* phosphorylation sites.

STE20 kinases are highly conserved in species and are likely to represent ancient ancestral kinases that tend to

operate as upstream kinases (Hanks and Hunter, 1995). It is tempting to speculate that activation of STE20 kinases by MO25 might represent an early mechanism that evolved to activate protein kinases. The assumption has always been that pseudokinases evolved from active protein kinases (Boudeau *et al*, 2006). However, it is possible that the opposite occurred, and that active protein kinases evolved from pseudokinases. Arguably, the minimum requirement for a protein to function like a kinase is to be capable of interacting with targets in a regulated manner. A pseudokinase that can be converted from a non-target binding open conformation to a closed active conformation capable of binding and influencing a target could represent a basic regulatory module that kinases evolved from. If the first active STE20 kinase molecules capable of phosphorylating substrates evolved from an MO25 and ATP-binding pseudokinase, this could explain why binding of MO25 has been retained as a regulatory mechanism for controlling a diverse subset of STE20 kinases.

Materials and methods

Reagents

Tissue-culture reagents were from Life Technologies. P81 phosphocellulose paper was from Whatman and [γ-^{32}P]-ATP was from Perkin Elmer. All peptides were synthesised by Pepceuticals. The Myelin basic protein (MBP) and siRNA oligonucleotides were from Sigma.

General methods and plasmids

Cloning, restriction enzyme digests, DNA ligations and other recombinant DNA procedures were performed using standard protocols. All mutagenesis reactions were performed using KOD polymerase (Novagen) followed by digestion of the product with *Dpn*I. All the clones were provided by the Division of Signal Transduction Therapy (DSTT), Dundee. The DNA accession numbers as well as the DSTT DNA code (DU) number for all kinases cloned for this study are listed in Supplementary Tables I and II. DNA constructs used for transfection were purified from DH5α strain of *E. coli* using Qiagen Plasmid kits according to the manufacturer's protocol. All DNA constructs were verified by DNA sequencing performed by DNA Sequencing & Services (MRCPPU, College of Life Sciences, University of Dundee, UK; www.dnaseq.co.uk) using Applied Biosystems Big-Dye Version 3.1 chemistry on an Applied Biosystems model 3730 automated capillary DNA sequencer. All protein concentrations were determined using a Bradford method kit (Bio-Rad). The purity of all proteins was assessed by SDS–polyacrylamide gel electrophoresis. Sequence alignments were performed using MUSCLE (Edgar, 2004), which were edited and displayed using the program ALINE (Bond and Schuttelkopf, 2009).

Buffers

HEK293 cell lysis buffer for mammalian cells: 50 mM Tris–HCl (pH 7.5), 1 mM EGTA, 1 mM EDTA, 1% (w/v) Non-idet P40, 1 mM sodium orthovanadate, 50 mM sodium fluoride, 5 mM sodium pyrophosphate, 0.27 M sucrose, 0.1% (v/v) 2-mercaptoethanol, 1 mM benzamidine and 0.1 mM PMSF. Bacterial lysis buffer: 50 mM Tris–HCl (pH 7.8), 150 mM NaCl, 0.27 M sucrose, 1 mM benzamidine, 1 mM EGTA, 1 mM EDTA, 0.1 mM PMSF and 0.01% (v/v) β-mercaptoethanol, supplemented with 0.5 mg/ml lysozyme and 0.3 mg/ml DNAse-I. MBS buffer contained 20 mM Mes/NaOH, pH 6.3, 140 mM NaCl, 40 mM KCl. Sf21 cell lysis buffer: 50 mM Tris–HCl, pH 7.8, 0.15 M NaCl, 5% (v/v) glycerol, 0.2 mM EDTA, 0.2 mM EGTA, 1 mM benzamidine, 0.2 mM PMSF, 5 μM leupeptine, 20 mM imidazole and 0.075% (v/v) β-mercaptoethanol. Low-salt buffer contained 50 mM Tris–HCl, pH 7.8, 150 mM NaCl, 5% (v/v) glycerol, 0.2 mM EDTA, 0.2 mM EGTA, 1 mM benzamidine, 20 mM imidazole and 0.075% (v/v) β-mercaptoethanol. Buffer A was 50 mM Tris–HCl (pH 7.5), 0.1 mM EGTA and 0.1% (v/v) 2-mercaptoethanol. The SDS sample buffer contains 50 mM Tris–HCl (pH 6.8), 1% (w/v) SDS, 10% (v/v) glycerol, 0.005% (w/v) bromophenol blue and 1% (v/v) 2-mercaptoethanol. TBS-T buffer contains 50 mM Tris–HCl (pH 7.5), 0.15 M NaCl and 0.25% (v/v) Tween. Basic control buffer contains 135 mM NaCl, 5 mM KCl, 0.5 mM $CaCl_2$, 0.5 mM $MgCl_2$, 0.5 mM Na_2HPO_4, 0.5 mM Na_2SO_4 and 15 mM HEPES (pH 7.0). Hypotonic low-chloride buffer contains 67.5 mM sodium gluconate, 2.5 mM potassium gluconate, 0.25 mM $CaCl_2$, 0.25 mM $MgCl_2$, 0.5 mM Na_2HPO_4, 0.5 mM Na_2SO_4 and 7.5 mM HEPES (pH 7.0).

Antibodies

The following antibodies were raised in sheep and affinity purified on the appropriate antigen: the SPAK/OSR1 (T-loop) phospho-Thr233/T185 (S240C), SPAK/OSR1 (S-motif) phospho-Ser373/S325 (S670B) were produced as reported previously (Zagorska *et al*, 2010). The anti-P-NKCC1 (S763B) was raised against a peptide containing the phosphorylated Thr203, Thr207 and Thr212 (Vitari *et al*, 2006). The MST4 (S831C) total antibody was raised against the full-length protein. The MO25β (S082B) antibody was raised against full-length GST-tagged MO25β (NCBI accession number AK022 639). The following antibodies were purchased from Cell Signaling: ERK1/2 (Total; cat. No. 9102), OSR1 (Total; cat. No. 3729) SPAK (Total; cat. No. 2281) and MO25α (Total; cat. No. 2716). Horseradish peroxidase (HRP)-conjugate anti-GST (ab58626) antibody was purchased from Abcam, and secondary antibodies coupled to HRP used for immunoblotting were obtained from Pierce Chemical Co. Preimmune IgG used in control immunoprecipitation experiments were affinity purified from preimmune serum using protein-G Sepharose.

Cell culture, transfections, stimulation and lysis

HEK 293 cells were cultured on 10 cm diameter dishes in 10 ml of DMEM supplemented with 10% (v/v) fetal bovine serum, 2 mM L-glutamine, 100 U/ml penicillin and 0.1 mg/ml streptomycin. For transfection experiments, 3–9 μg of DNA was mixed with 20 μl of 1 mg/ml polyethylenimine (Polysciences) in 1 ml of plain DMEM for each dish. The mixture was left to stand for 30 min and added onto the cells. Cells were then lysed 36 h post-transfection in 1 ml of ice-cold lysis buffer. Cell lysates were clarified by centrifugation at 20 000 *g* for 15 min at 4°C, and the supernatants divided into aliquots, frozen in liquid nitrogen, and stored at −20°C.

Protein expression and assay

Details of protein expression, affinity tags used for purification and assay conditions are summarised in Supplementary Table II.

Expression of proteins in HEK293 cells

Ten cm diameter dishes of 293 cells were transiently transfected as described above with 3 μg of the pEBG-2T constructs encoding N-terminal GST fusions of wild-type and mutant STE20 kinase. Cells were lysed 36 h post-transfection, and the clarified lysates were incubated for 1 h on a rotating platform with glutathione-Sepharose (GE Healthcare; 10 μl/dish of lysate) previously equilibrated in lysis buffer. The beads were washed once with lysis buffer containing 0.15 M NaCl, three times with lysis buffer containing 0.5 M NaCl and twice with buffer A. The proteins were eluted from the resin by incubation with the same buffer A containing 0.27 M sucrose and 20 mM of reduced glutathione (pH 7.5). The beads were then removed by filtration through a 0.44 mm filter, and the eluted protein aliquoted and stored at −80°C.

Expression of proteins in E. coli

Cells transformed with the appropriate expression plasmid were grown in Luria Bertani medium to $A_{600} = 0.7$ at 37°C. Protein expression was induced by the addition of 0.25 mM isopropyl β-D-1-thiogalactopyranoside and cells incubated for a further 16 h at 26°C. Cells were harvested by centrifugation for 30 min at 3500 *g* and resuspended in ice-cold bacteria lysis buffer. Cells were lysed by sonication (10 × 10 s pulses), clarified by centrifugation at 26 000 *g* and lysates incubated for 1 h on a rotating platform with glutathione-Sepharose (1 ml/l of *E. coli* culture) pre-equilibrated in bacterial lysis buffer. The beads were then washed with 10 column volumes (CVs) of bacterial lysis buffer lacking DNase-1 and lysozyme and a further 50 CVs of high-salt wash buffer containing 0.5 M NaCl. Beads were re-equilibrated in 10 CVs of wash buffer, and the proteins were eluted by either incubating with PreScission protease (15 μg/mg of protein) for 16 h or with 20 mM reduced

glutathione (See Supplementary Table II). Protein eluates were divided into aliquots and stored at −80°C. For SPR analysis, the proteins were eluted in wash buffer without sucrose.

Expression of proteins in insect cells

Standard methods were used to generate recombinant progeny 2 (P2) baculoviruses expressing each kinase with epitope tags summarised in Supplementary Table II. These cultures were used (1:10) to infect 600 ml of Sf21 cells cultured in suspension. After 48 h infection, cells were harvested and washed in MBS buffer, before lysing in ice-cold Sf21 lysis buffer. Lysates were clarified by centrifugation at 26 000 *g* for 30 min. For 6-His-tagged proteins, the supernatant was incubated on a rolling platform for 1 h at 4°C with 0.3 ml of NiNTA agarose beads (Qiagen), pre-equilibrated in low-salt buffer. The beads were washed with 10 CV of low-salt buffer and 60 CV of high-salt buffer (low-salt buffer containing 0.5 M NaCl), followed by 10 CV of low-salt buffer. The protein was eluted with 10 CV of low-salt buffer supplemented with 0.1 M imidazole. The purification of MBP tagged proteins was similar to the 6-His-tagged purification, except that amylose resin replaced the NiNTA agarose and purified recombinant protein eluted with 12 mM maltose.

Assaying STE-family kinases by measuring the phosphorylation of specific substrates

The activity of recombinant STE-family kinases was assayed by using specific substrates and at the concentration summarised in Supplementary Table II. Phosphotransferase activity of each kinase was measured in a total assay volume of 50 µl consisting of 50 mM Tris–HCl (pH 7.5), 0.1 mM EGTA, 0.1% (v/v) 2-mercaptoethanol, 10 mM magnesium acetate, 0.1 mM [γ-32P]ATP (200 c.p.m./pmol) and the reported amount of substrate (Supplementary Table II). The assays were carried out at 30°C and were terminated after 15 min by applying 40 µl of the reaction mixture onto P81 membranes. These were washed in phosphoric acid, and the incorporated radioactivity was measured by scintillation counting as described previously for MAP kinase (Alessi *et al*, 1995). One unit (U) of activity represents the incorporation to the substrate of 1 nmol of γ-32P per minute. For the enzymes that need to be activated, a pre-incubation with GST-c-Raf [1-306] Y340D Y341D (for GST-MAP2K1) or His-MEKK1 (for MAP2K2, MAP2K3, MAP2K4 MAP2K6 and MAP2K7) for 30 min at 30°C was performed in a buffer containing 50 mM Tris–HCl (pH 7.5), 0.1 mM EGTA, 0.1% (v/v) 2-mercaptoethanol, 10 mM magnesium acetate and 0.1 mM ATP. After the activation steps, the enzymes were re-purified before performing the kinase assay.

Immunoblotting

Twenty µg of cell lysates, 0.2–1 µg of purified proteins or immunoprecipitates in SDS sample buffer were subjected to electrophoresis on a polyacrylamide gel and transferred to nitrocellulose membranes. The membranes were incubated for 1 h with TBS-T containing either 10% (w/v) skimmed milk powder (for antibodies raised in sheep) or 5% (w/v) BSA (for all other antibodies). The membranes were then immunoblotted in the same buffer for 2 h at room temperature with the indicated primary antibodies. Sheep antibodies were used at a concentration of 0.5–1 µg/ml, whereas commercial antibodies were diluted to 1000-fold. The incubation with phosphospecific sheep antibodies was performed with the addition of 10 µg/ml of the dephosphopeptide antigen used to raise the antibody. The blots were then washed six times with TTBS and incubated with secondary HRP-conjugated antibodies in 5% skimmed milk. After repeating the washing steps, the signal was detected with the enhanced chemiluminescence reagent. Immunoblots were developed using a film automatic processor (SRX-101; Konica Minolta Medical), and films were scanned with a 300-dp1 resolution on a scanner (PowerLook 1000; UMAX).

siRNA for MO25α

Two siRNA duplex targeting MO25α (siMO25α oligo-1: 5′-GCAUUUGCUGUUAGCUAUU-3′; siMO25α oligo-2: 5′-CACUCUUAU UGAUUCAUGA-3′) and scramble duplex (5′-CCUACUAAGCGACACC AU-3′) were transfected in HEK293 cells with HiperFect (Qiagen) at concentration of 100 nM, according to the manufacturer's instructions. Oligo-1 and oligo-2 target non-coding regions of MO25α. HEK293 cells were plated at confluence of 4×10^5 cells/well in six-well plates (3.4 cm diameter/well) and transfected with the siMO25α oligo-1 950 nM) and/or oligo-2 (50 nM each) or scrambled duplex (50–100 nM). After 24 h siRNA transfection, Myc-tagged MO25α (3 µg) was transfected using the polyethylenimine method (Durocher *et al*, 2002). After 72 h siRNA transfection, cells were treated for 5 min with Basic or Hypotonic solution and lysed as described before (Richardson *et al*, 2008).

^{86}Rb uptake assay in HEK293 cells

HEK293 cells were plated at a confluence of 1.5×10^5 cells/well in 12-well plates (2.4 cm diameter/well) and transfected with the siMO25α oligo-1 and oligo-2 together or scramble duplex. The ^{86}Rb uptake assay was performed on the cells 72 h post-transfection. Culture media was removed from the wells and replaced with either basic control or hypotonic low-chloride medium for 5 or 10 min. Medium was removed and replaced with either basic or hypotonic low-chloride medium plus 1 mM ouabain in the presence or absence of 0.1 mM bumetanide for further 5 min. After this period, cells were washed twice with isotonic uptake medium containing the same additives (ouabain ± bumetanide). Following washing, cells were incubated with isotonic uptake media containing 4 µCi/ml of ^{86}Rb for 5 min. After this period, cells were rapidly washed three times with ice-cold non-radioactive medium. The cells were lysed in 300 µl of ice-cold lysis buffer and ^{86}Rb-uptake quantified on a Perkin Elmer liquid scintillation analyzer.

SPR measurements of STE20 kinases binding to MO25α

SPR measurements were performed using a BIAcore T100 instrument. SPAK, OSR1 and MST4 were immobilised on a CM5 sensor chip using standard amine-coupling chemistry, and 10 mM HBS (pH 7.4) was used as the running buffer. The carboxymethyl dextran surface was activated with a 7 min injection of a 1:1 ratio of 0.4 M 1-ethyl-3-(3-dimethylaminopropyl) carbodiimide hydrochloride/0.1 M *N*-hydroxy succinimide. The STE20 kinases (5–7 µM) were coupled to the surface with a 1-min injection of protein diluted in 10 mM sodium acetate (pH 5.5). Remaining activated groups were blocked with a 7 min injection of 1 M ethanolamine (pH 8.5). The kinases were immobilised on three flow cells of a CM5 chip at densities 1000–3000 RU performed at 25°C, leaving one flow cell as a reference to subtract any possible nonspecific binding. The wild-type and mutant forms of MO25α where prepared in running buffer containing 50 mM Tris (pH 7.5), 0.15 mM NaCl, 1 mM DTT, 0.005% P20, and 0.1 mg/ml BSA in the presence of 0.1 mM ATP and 1 mM $MgCl_2$, and injected over all four surfaces at concentration series over the range of 0.2–100 µM. Each concentration was injected in duplicate over all surfaces. Association was measured for 30 s at a flow rate of 50 µl/min, and dissociation was measured for 1 min. MO25α dissociated completely from the STE20 kinase surfaces, thus eliminating the need for a regeneration step. Data were double referenced to the reference surface to subtract any possible nonspecific binding and to the blank buffer injections to subtract drift of the target from surface. Data were fitted to a 1:1 (Hill slope = 1) or 2:1 binding site model where appropriate (Hill slope <0.7). Equilibrium constants (K_d) were calculated from a saturation binding curve by fitting the measured response (R) from specific binding to the following equations: $R = R_{max}[STE20K]/([STE20K] + K_d)$ was used for a 1:1 binding model and $R = (R_{max1}[STE20K]/([STE20K] + K_{d1})) + (R_{max2}[STE20K]/([STE20K] + K_{d2}))$ were used for a 2:1 binding model. R_{max1} and R_{max2} are the relative maximal changes in response for sites 1 and 2, respectively, and K_{d1} and K_{d2} are the equilibrium dissociation constants for sites 1 and 2, respectively. Dose–response curves for calculating the Hill slope (H) of the data were fitted with the following equation: $R = \text{minimum} + (\text{maximum} - \text{minimum})/(1 + 10^{((\log EC50 - [STE20K]) \times H)})$. All data were analysed using the GraphPad-PRISM software.

Supplementary data

Supplementary data are available at *The EMBO Journal* Online (http://www.embojournal.org).

Acknowledgements

We are grateful to Kei Sakamoto for undertaking the immunoblot analysis of MO25 expression in different tissues (Supplementary Figure S14) as well as Eric Weiss (Northwestern University, IL, USA) and Ciaran Richardson for valuable discussions. We thank the staff at the Sequencing Service (School of Life Sciences, University of

Dundee, Scotland) for DNA sequencing and the protein production and antibody purification teams (Division of Signal Transduction Therapy (DSTT), University of Dundee) co-ordinated by Hilary McLauchlan and James Hastie for expression and purification of antibodies. We thank the Medical Research Council and the pharmaceutical companies supporting the DSTT Unit (AstraZeneca, Boehringer-Ingelheim, GlaxoSmithKline, Merck-Serono and Pfizer) for financial support.

Conflict of interest

The authors declare that they have no conflict of interest.

References

Alessi DR, Cohen P, Ashworth A, Cowley S, Leevers SJ, Marshall CJ (1995) Assay and expression of mitogen-activated protein kinase, MAP kinase kinase, and Raf. *Methods Enzymol* **255:** 279–290

Alessi DR, Sakamoto K, Bayascas JR (2006) LKB1-dependent signaling pathways. *Annu Rev Biochem* **75:** 137–163

Baas AF, Boudeau J, Sapkota GP, Smit L, Medema R, Morrice NA, Alessi DR, Clevers HC (2003) Activation of the tumour suppressor kinase LKB1 by the STE20-like pseudokinase STRAD. *EMBO J* **22:** 3062–3072

Bidlingmaier S, Weiss EL, Seidel C, Drubin DG, Snyder M (2001) The Cbk1p pathway is important for polarized cell growth and cell separation in *Saccharomyces cerevisiae*. *Mol Cell Biol* **21:** 2449–2462

Bond CS, Schuttelkopf AW (2009) ALINE: a WYSIWYG protein-sequence alignment editor for publication-quality alignments. *Acta Crystallogr D Biol Crystallogr* **65**(Part 5)**:** 510–512

Boudeau J, Baas AF, Deak M, Morrice NA, Kieloch A, Schutkowski M, Prescott AR, Clevers HC, Alessi DR (2003a) MO25alpha/beta interact with STRADalpha/beta enhancing their ability to bind, activate and localize LKB1 in the cytoplasm. *EMBO J* **22:** 5102–5114

Boudeau J, Deak M, Lawlor MA, Morrice NA, Alessi DR (2003b) Heat-shock protein 90 and Cdc37 interact with LKB1 and regulate its stability. *Biochem J* **370**(Part 3)**:** 849–857

Boudeau J, Miranda-Saavedra D, Barton GJ, Alessi DR (2006) Emerging roles of pseudokinases. *Trends Cell Biol* **16:** 443–452

Boudeau J, Scott JW, Resta N, Deak M, Kieloch A, Komander D, Hardie DG, Prescott AR, van Aalten DM, Alessi DR (2004) Analysis of the LKB1-STRAD-MO25 complex. *J Cell Sci* **117:** 6365–6375

Dan I, Watanabe NM, Kusumi A (2001) The Ste20 group kinases as regulators of MAP kinase cascades. *Trends Cell Biol* **11:** 220–230

Darman RB, Forbush B (2002) A regulatory locus of phosphorylation in the N terminus of the Na-K-Cl cotransporter, NKCC1. *J Biol Chem* **277:** 37542–37550

Durocher Y, Perret S, Kamen A (2002) High-level and high-throughput recombinant protein production by transient transfection of suspension-growing human 293-EBNA1 cells. *Nucleic Acids Res* **30:** E9

Edgar RC (2004) MUSCLE: a multiple sequence alignment method with reduced time and space complexity. *BMC Bioinformatics* **5:** 113

Elbing K, McCartney RR, Schmidt MC (2006) Purification and characterization of the three Snf1-activating kinases of *Saccharomyces cerevisiae*. *Biochem J* **393**(Part 3)**:** 797–805

Gimenez I, Forbush B (2005) Regulatory phosphorylation sites in the NH2 terminus of the renal Na-K-Cl cotransporter (NKCC2). *Am J Physiol Renal Physiol* **289:** F1341–F1345

Godlewski J, Nowicki MO, Bronisz A, Nuovo G, Palatini J, De Lay M, Van Brocklyn J, Ostrowski MC, Chiocca EA, Lawler SE (2010) MicroRNA-451 regulates LKB1/AMPK signaling and allows adaptation to metabolic stress in glioma cells. *Mol Cell* **37:** 620–632

Goshima T, Kume K, Koyano T, Ohya Y, Toda T, Hirata D (2010) Fission yeast germinal center (GC) kinase Ppk11 interacts with Pmo25 and plays an auxiliary role in concert with the morphogenesis Orb6 network (MOR) in cell morphogenesis. *J Biol Chem* **285:** 35196–35205

Hanks SK, Hunter T (1995) Protein kinases 6. The eukaryotic protein kinase superfamily: kinase (catalytic) domain structure and classification. *FASEB J* **9:** 576–596

Hawley SA, Boudeau J, Reid JL, Mustard KJ, Udd L, Makela TP, Alessi DR, Hardie DG (2003) Complexes between the LKB1 tumor suppressor, STRADalpha/beta and MO25alpha/beta are upstream kinases in the AMP-activated protein kinase cascade. *J Biol* **2:** 28

Hedbacker K, Carlson M (2008) SNF1/AMPK pathways in yeast. *Front Biosci* **13:** 2408–2420

Jeffrey PD, Russo AA, Polyak K, Gibbs E, Hurwitz J, Massagué J, Pavletich NP (1995) Mechanism of CDK activation revealed by the structure of a cyclinA-CDK2 complex. *Nature* **376:** 313–320

Kanai M, Kume K, Miyahara K, Sakai K, Nakamura K, Leonhard K, Wiley DJ, Verde F, Toda T, Hirata D (2005) Fission yeast MO25 protein is localized at SPB and septum and is essential for cell morphogenesis. *EMBO J* **24:** 3012–3025

Karos M, Fischer R (1999) Molecular characterization of HymA, an evolutionarily highly conserved and highly expressed protein of Aspergillus nidulans. *Mol Gen Genet* **260:** 510–521

Ko TP, Jeng WY, Liu CI, Lai MD, Wu CL, Chang WJ, Shr HL, Lu TJ, Wang AH (2010) Structures of human MST3 kinase in complex with adenine, ADP and Mn2 + . *Acta Crystallogr D Biol Crystallogr* **66**(Part 2)**:** 145–154

Lee SJ, Cobb MH, Goldsmith EJ (2009) Crystal structure of domain-swapped STE20 OSR1 kinase domain. *Protein Sci* **18:** 304–313

Lizcano JM, Goransson O, Toth R, Deak M, Morrice NA, Boudeau J, Hawley SA, Udd L, Makela TP, Hardie DG, Alessi DR (2004) LKB1 is a master kinase that activates 13 kinases of the AMPK subfamily, including MARK/PAR-1. *EMBO J* **23:** 833–843

Manning G, Whyte DB, Martinez R, Hunter T, Sudarsanam S (2002) The protein kinase complement of the human genome. *Science* **298:** 1912–1934

Milburn CC, Boudeau J, Deak M, Alessi DR, van Aalten DM (2004) Crystal structure of MO25 alpha in complex with the C terminus of the pseudo kinase STE20-related adaptor. *Nat Struct Mol Biol* **11:** 193–200

Miyamoto H, Matsushiro A, Nozaki M (1993) Molecular cloning of a novel mRNA sequence expressed in cleavage stage mouse embryos. *Mol Reprod Dev* **34:** 1–7

Nelson B, Kurischko C, Horecka J, Mody M, Nair P, Pratt L, Zougman A, McBroom LD, Hughes TR, Boone C, Luca FC (2003) RAM: a conserved signaling network that regulates Ace2p transcriptional activity and polarized morphogenesis. *Mol Biol Cell* **14:** 3782–3803

Nozaki M, Onishi Y, Togashi S, Miyamoto H (1996) Molecular characterization of the Drosophila Mo25 gene, which is conserved among Drosophila, mouse, and yeast. *DNA Cell Biol* **15:** 505–509

Ponce-Coria J, San-Cristobal P, Kahle KT, Vazquez N, Pacheco-Alvarez D, de Los Heros P, Juarez P, Munoz E, Michel G, Bobadilla NA, Gimenez I, Lifton RP, Hebert SC, Gamba G (2008) Regulation of NKCC2 by a chloride-sensing mechanism involving the WNK3 and SPAK kinases. *Proc Natl Acad Sci USA* **105:** 8458–8463

Rafiqi FH, Zuber AM, Glover M, Richardson C, Fleming S, Jovanovic S, Jovanovic A, O'Shaughnessy KM, Alessi DR (2010) Role of the WNK-activated SPAK kinase in regulating blood pressure. *EMBO Mol Med* **2:** 63–75

Record CJ, Chaikuad A, Rellos P, Das S, Pike AC, Fedorov O, Marsden BD, Knapp S, Lee WH (2010) Structural comparison of human mammalian ste20-like kinases. *PLoS One* **5:** e11905

Richardson C, Alessi DR (2008) The regulation of salt transport and blood pressure by the WNK-SPAK/OSR1 signalling pathway. *J Cell Sci* **121**(Part 20)**:** 3293–3304

Richardson C, Rafiqi FH, Karlsson HK, Moleleki N, Vandewalle A, Campbell DG, Morrice NA, Alessi DR (2008) Activation of the thiazide-sensitive Na + -Cl- cotransporter by the WNK-regulated kinases SPAK and OSR1. *J Cell Sci* **121**(Part 5)**:** 675–684

Richardson C, Sakamoto K, de Los Heros P, Deak M, Campbell DG, Prescott AR, Alessi DR (2011) Regulation of the NKCC2 ion

cotransporter by SPAK-OSR1-dependent and -independent pathways. *J Cell Sci* **124**(Part 5)**:** 789–800

Stegert MR, Hergovich A, Tamaskovic R, Bichsel SJ, Hemmings BA (2005) Regulation of NDR protein kinase by hydrophobic motif phosphorylation mediated by the mammalian Ste20-like kinase MST3. *Mol Cell Biol* **25:** 11019–11029

ten Klooster JP, Jansen M, Yuan J, Oorschot V, Begthel H, Di Giacomo V, Colland F, de Koning J, Maurice MM, Hornbeck P, Clevers H (2009) Mst4 and Ezrin induce brush borders downstream of the Lkb1/Strad/Mo25 polarization complex. *Dev Cell* **16:** 551–562

Villa F, Deak M, Alessi DR, van Aalten DM (2008) Structure of the OSR1 kinase, a hypertension drug target. *Proteins* **73:** 1082–1087

Vitari AC, Deak M, Morrice NA, Alessi DR (2005) The WNK1 and WNK4 protein kinases that are mutated in Gordon's hypertension syndrome phosphorylate and activate SPAK and OSR1 protein kinases. *Biochem J* **391**(Part 1)**:** 17–24

Vitari AC, Thastrup J, Rafiqi FH, Deak M, Morrice NA, Karlsson HK, Alessi DR (2006) Functional interactions of the SPAK/OSR1 kinases with their upstream activator WNK1 and downstream substrate NKCC1. *Biochem J* **397:** 223–231

Yang SS, Lo YF, Wu CC, Lin SW, Yeh CJ, Chu P, Sytwu HK, Uchida S, Sasaki S, Lin SH (2010) SPAK-knockout mice manifest Gitelman syndrome and impaired vasoconstriction. *J Am Soc Nephrol* **21:** 1868–1877

Yang SS, Morimoto T, Rai T, Chiga M, Sohara E, Ohno M, Uchida K, Lin SH, Moriguchi T, Shibuya H, Kondo Y, Sasaki S, Uchida S (2007) Molecular pathogenesis of pseudohypoaldosteronism type II: generation and analysis of a Wnk4(D561A/+) knockin mouse model. *Cell Metab* **5:** 331–344

Zagorska A, Deak M, Campbell DG, Banerjee S, Hirano M, Aizawa S, Prescott AR, Alessi DR (2010) New roles for the LKB1-NUAK pathway in controlling myosin phosphatase complexes and cell adhesion. *Sci Signal* **3:** ra25

Zagorska A, Pozo-Guisado E, Boudeau J, Vitari AC, Rafiqi FH, Thastrup J, Deak M, Campbell DG, Morrice NA, Prescott AR, Alessi DR (2007) Regulation of activity and localization of the WNK1 protein kinase by hyperosmotic stress. *J Cell Biol* **176:** 89–100

Zeqiraj E, Filippi BM, Deak M, Alessi DR, van Aalten DM (2009a) Structure of the LKB1-STRAD-MO25 complex reveals an allosteric mechanism of kinase activation. *Science* **326:** 1707–1711

Zeqiraj E, Filippi BM, Goldie S, Navratilova I, Boudeau J, Deak M, Alessi DR, van Aalten DM (2009b) ATP and MO25alpha regulate the conformational state of the STRADalpha pseudokinase and activation of the LKB1 tumour suppressor. *PLoS Biol* **7:** e1000126

Zhang X, Gureasko J, Shen K, Cole PA, Kuriyan J (2006) An allosteric mechanism for activation of the kinase domain of epidermal growth factor receptor. *Cell* **125:** 1137–1149